

Properties of interstellar wind leading to shape morphology of the dust surrounding HD 61005

P. Pástor

Tekov Observatory, Sokolovská 21, 934 01 Levice, Slovak Republic
e-mail: pavol.pastor@hvezdarenlevice.sk

ABSTRACT

Aims. A structure formed by dust particles ejected from debris ring around HD 61005 is observed in the scattered light. Our aim is to constrain interstellar wind parameters that lead to shape morphology in the vicinity of HD 61005 using currently available observational data for the debris ring.

Methods. We solved equation of motion of 2×10^5 dust particles ejected from the debris ring under the action of the electromagnetic radiation, stellar wind and interstellar wind. We applied 2D grid observed from given direction for accumulation of the light scattered on the dust particles in order to determine the shape morphology.

Results. We determined groups of unknown properties of the interstellar wind that create the observed morphology. A relation between densities of gas components in the interstellar wind and its relative velocity is found. When the interstellar wind velocity is tilted from debris ring axis a simple relation between the properties of the interstellar wind and an angle between the line of sight and the interstellar wind velocity exists. Dust particles that are most significantly influenced by stellar radiation move on the boundary of observed structure.

Conclusions. We can conclude that observed structure at HD 61005 can be explained as a result of dust particles moving under the action of the interstellar wind. Required densities or velocities of the interstellar wind are much higher than that of the interstellar wind entering to the Solar system.

Key words. Protoplanetary disks – Interplanetary medium – ISM: individual objects: HD 61005 – Celestial mechanics

1. Introduction

An amount of dust sufficient to produce significant infrared excess was discovered at HD 61005 during *Spitzer* FEPS survey. The star was selected by Hines et al. (2007) as promising target for *HST* NICMOS observations. In the scattered light they resolved a asymmetric structure of dust at the star. Hines et al. (2007) suggested that the observed morphology could be formed as a result of an interaction between dust particles originating in the system and a gas from an interstellar medium (ISM) moving with respect to the star (interstellar wind). The fact that the star's proper motion roughly points north (van Leeuwen 2007), while the disk's swept-back "wings" are directed to the south, might be more than just a coincidence (Hines et al. 2007; Esposito et al. 2016). A result of the interaction was obtained numerically in Debes et al. (2009). They used a debris ring ejecting dust particles on unbound orbits varying further due to the interstellar wind (ISW) and the stellar gravity reduced by Keplerian term from Poynting–Robertson (PR) effect. Maness et al. (2009) used dust particles on bound orbits interacting with the ISM gas in order to obtain the observed morphology. Their results were based on a secular variation of dust orbits due to the ISM gas taken from Scherer (2000). According to results in Scherer (2000) the dust particles on bound orbits should undergo an increase of the semimajor axis due to the acceleration from the ISW. The increase of the semimajor axis should create the observed swept-back structure in Maness et al. (2009). However, in Pástor et al. (2011) and Pástor (2012b) was

analytically proved that for the dust particles on bound orbits the semimajor axis always decrease independently of an orientation of the orbit with respect to the interstellar gas velocity vector.

The debris ring ejecting the dust particles was resolved in the scattered light by Buenzli et al. (2010). According to the observations the bulk of the debris ring with low eccentricity is roughly located between 55 and 65 AU from HD 61005 with an apparent inclination 5.7 from edge-on Buenzli et al. (2010). Esposito et al. (2016) suggested that dust asymmetry observed at HD 61005 can be explained as result of secular perturbations of dust particles on bound orbits by an eccentric and inclined planet. Such a explanation requires smooth boundaries at the ends of the swept-back structure (due to the bound orbits) and that is not observed as far as 350 AU from the star (Schneider et al. 2014). Moreover, scattering behaviour is more consistent with smaller particles below blow-out radius (Hines et al. 2007).

In this study we use observed properties of the debris ring at HD 61005 in order to explain observed asymmetric morphology using interaction of the dust particles on unbound orbits with the ISW. We concentrate on groups of unknown properties of the ISM gas which lead to the observed morphology. We take further Debes et al. (2009) results by using of the observed dimensions of the debris ring and by using of correct acceleration of the dust particles caused by the ISW.

2. Model

HD 61005 is G8V star with visual magnitude 8.22 at 35.4 pc. Its position and kinematics with respect to the Sun is typical for members of the Argus association (Desidera et al. 2011). Stellar age of the Argus association is believed to be 40 Myr (Torres et al. 2008). The optical and near infrared (IR) photometry measurements suggest that star has temperature similar to our Sun. In far-IR the star shows IR-excess from the debris disk observed also in the scattered light (e.g. Schneider et al. 2014). We verified stellar parameters from Olofsson et al. (2016) and use them in this study. The luminosity and radius of the star used are $L_\star = 0.58 L_\odot$ and $R_\star = 0.84 R_\odot$, respectively. For the age 40 Myr and an effective temperature of 5500 K (used to scale the photometry with Kurucz library) isochrones from Siess et al. (2000) give the stellar mass $1.1 M_\odot$. Thus, HD 61005 is considered as a pre-main-sequence star.

2.1. Electromagnetic radiation

The acceleration of moving spherical dust particle caused by the electromagnetic radiation is the PR effect (Poynting 1904; Robertson 1937; Klačka 1992, 2004; Klačka et al. 2014). The acceleration is

$$\frac{d\mathbf{v}}{dt} = \frac{\mu\beta}{r^2} \left[\left(1 - \frac{\mathbf{v} \cdot \mathbf{e}_R}{c} \right) \mathbf{e}_R - \frac{\mathbf{v}}{c} \right], \quad (1)$$

where $\mu = GM_\star$, G is the gravitational constant, M_\star is the mass of the star, r is the stellocentric distance, \mathbf{e}_R is the radial unit vector directed from the star to the dust particle, \mathbf{v} is the velocity of the particle with respect to the star, and c is the speed of light. The parameter β is defined as the ratio between the electromagnetic radiation pressure force and the gravitational force between the star and the particle at rest with respect to the star

$$\beta = \frac{L_\star \bar{Q}'_{\text{pr}} A'}{4\pi c \mu m}. \quad (2)$$

Here, L_\star is the stellar luminosity, \bar{Q}'_{pr} is the dimensionless efficiency factor for the radiation pressure averaged over the stellar spectrum and calculated for the radial direction ($\bar{Q}'_{\text{pr}} = 1$ for a perfectly absorbing sphere), c is the speed of light in vacuum, and A' is the geometric cross-section of the particle with mass m .

2.2. Mass loss rate

The solar heliosphere is created in an interaction of the solar wind with the ISM gas incoming to the Solar system. Also in the vicinity of HD 61005 its stellar wind will be influenced by an incoming ISM gas. Far outside of the astrophere of HD 61005 we may neglect an acceleration of dust particles caused by the stellar wind (e.g. Richardson et al. 2008). For correct description of the stellar wind at HD 61005 we need to know also mass loss rate of this star. Recent results in Johnstone et al. (2015) enable approximately determine mass loss rate for stars of masses between $0.4 M_\odot$ and $1.1 M_\odot$ if we know the angular velocity of surface rotation, the radius and the mass of the star. Unfortunately, the authors considered in their sample only stars older than 100 Myr to fit parameters. Although, their theory enables consideration also of the pre-main-sequence stars. The relation for

the wind torque in Matt et al. (2012) was originally derived also for pre-main-sequence stars and did not lose this applicability. Also the relation for dependence of the X-ray flux as a function of the stellar mass and the rotation period from Wright et al. (2011) is applicable for younger stars. Improve their fit for younger stars is behind scope of this study. In order to determine the mass loss rate for HD 61005 we will simply assume that fit obtained in Johnstone et al. (2015) can be used for this star. We will see later that the astrophere of HD 61005 will be far inside of the debris ring also for much larger mass loss rates and stellar wind speeds. Stellar rotation with period $P_\star = 5.04$ days has been determined for HD 61005 in Desidera et al. (2011) from photometric measurements. This corresponds to the angular velocity of surface rotation $\Omega_\star = 2\pi/P_\star \approx 1.4 \times 10^{-5}$ rad/s. For stable stars rotating with higher than a saturation angular velocity the mass loss rate cannot be higher (e.g. Pallavicini et al. 1981; Wright et al. 2011). The saturation angular velocity for HD 61005 can be determined from Eq. 6 in Johnstone et al. (2015) as $\Omega_{\text{sat}} \approx 5.0 \times 10^{-5}$ rad/s. Since the obtained angular velocity of rotation for HD 61005 is below the saturation limit, the star is in unsaturated regime. The angular velocity of surface rotation coupled with $R_\star = 0.84 R_\odot$ and $M_\star = 1.1 M_\odot$ give using Eq. 4 in Johnstone et al. (2015) the mass loss rate $\dot{M}_\star \approx 4.8 \dot{M}_\odot$.

2.3. Stellar wind

Impinging particles of the stellar wind cause an acceleration of the dust particle that can be determined from a covariant equation of motion (Klačka et al. 2012)

$$\frac{d\mathbf{v}}{dt} = \frac{\mu\beta\eta u}{c\bar{Q}'_{\text{pr}} r^2} \left[\left(1 - \frac{\mathbf{v} \cdot \mathbf{e}_R}{u} \right) \mathbf{e}_R - \frac{\mathbf{v}}{u} \right], \quad (3)$$

where u is the speed of the stellar wind, η is the ratio of the stellar wind energy to the stellar electromagnetic radiation energy, both radiated per unit time. For η we can write

$$\eta = \frac{\dot{M}_\star c^2}{L_\star}. \quad (4)$$

Since HD 61005 is in the unsaturated regime for the speed of the stellar wind we obtain according to Johnstone et al. (2015) $u \approx 1200$ km/s. Using the mass loss rate of HD 61005 we obtain $\eta \approx 2.4$. Now, if we compare the Keplerian terms in Eqs. (1) and (3), we can neglect the Keplerian terms in Eq. (3) with respect to the Keplerian term in Eq. (1) for dust particles with $\bar{Q}'_{\text{pr}} = 1$.

2.4. ISW

Asymmetric structure observed at HD 61005 is commonly explained as result of an ISM gas affecting the dynamics of dust particles originating in the system (e.g. Debes et al. 2009; Maness et al. 2009). The acceleration used in Debes et al. (2009) was adopted from meteor theory and therefore have different handling with drag coefficients not very suitable for the ISM gas. In this work we use correct form acceleration caused the ISM gas influencing the dynamics of a spherical particle. The acceleration of the spherical dust

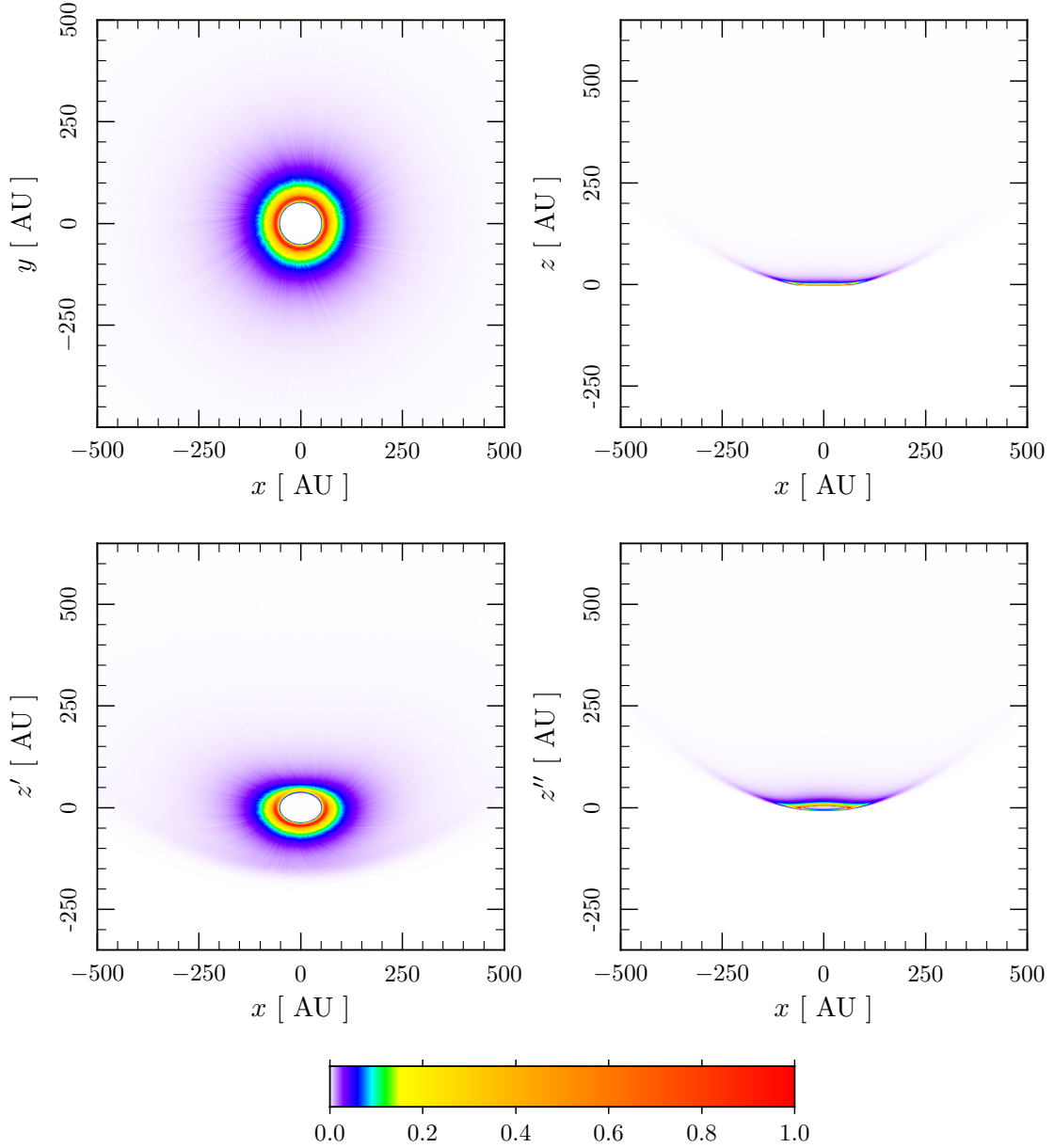


Fig. 1. An interaction of dust particles with $R = 0.168$, $\varrho = 1 \text{ g.cm}^{-3}$ and $\bar{Q}'_{\text{pr}} = 1.663$ ejected from parent bodies in the debris ring around HD 61005 located between 55 and 65 AU and the interstellar wind with densities $n_{\text{H}} = 80 \text{ cm}^{-3}$, $n_{\text{He}} = 6 \text{ cm}^{-3}$ and $n_{\text{p}} = 12.8 \text{ cm}^{-3}$ moving perpendicularly to the debris ring with relative velocity 30 km/s with respect to the star. Color scale is linear with observed intensity of light with wavelength $\lambda = 580 \text{ nm}$ scattered on the dust particles according to Mie scattering theory. The ring mid-plane is located in the xy -plane. The bottom-left plot is created by a rotation of a viewpoint in the top-left plot by the angle 45° counterclockwise around x -axis in yz -plane. The bottom-right plot is created by the rotation of a viewpoint in the top-left plot by the angle 95.7° counterclockwise around x -axis in yz -plane in order to show the shape morphology observed from the Earth.

moving through gas is (Baines et al. 1965)

$$\frac{d\mathbf{v}}{dt} = - \sum_{i=1}^N c_{\text{Di}} \gamma_i |\mathbf{v} - \mathbf{v}_{\text{F}}| (\mathbf{v} - \mathbf{v}_{\text{F}}) . \quad (5)$$

The sum in Eq. (5) runs over all particle species i . \mathbf{v}_{F} is the velocity of the ISM with respect to the star. c_{Di} in Eq. (5)

is the drag coefficient

$$c_{\text{Di}}(s_i) = \frac{1}{\sqrt{\pi}} \left(\frac{1}{s_i} + \frac{1}{2s_i^3} \right) e^{-s_i^2} + \left(1 + \frac{1}{s_i^2} - \frac{1}{4s_i^4} \right) \text{erf}(s_i) + (1 - \delta_i) \left(\frac{T_{\text{d}}}{T_i} \right)^{1/2} \frac{\sqrt{\pi}}{3s_i} , \quad (6)$$

where $\text{erf}(s_i)$ is the error function $\text{erf}(s_i) = 2/\sqrt{\pi} \int_0^{s_i} e^{-t^2} dt$, δ_i is the fraction of impinging particles specularly reflected at the surface (a diffuse reflection is assumed for the rest of the particles, see Baines et al. 1965; Gustafson 1994), T_{d} is

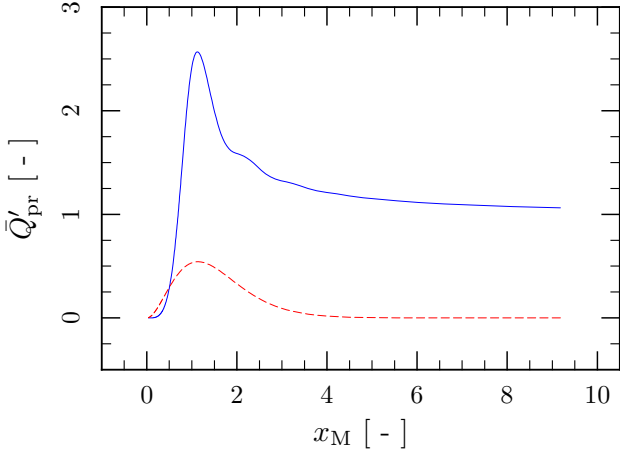


Fig. 2. Dimensionless efficiency factor for the radiation pressure (Q'_{pr}) determined for totally reflecting particle (solid line). Spectral distribution of Planck's blackbody with temperature 5500 K in dependence on $x_M = 2\pi R/\lambda$ for $R = 0.168 \mu\text{m}$ is shown for comparison (dashed line). The maximal Q'_{pr} is obtained for the dust particle with $R = 0.168 \mu\text{m}$.

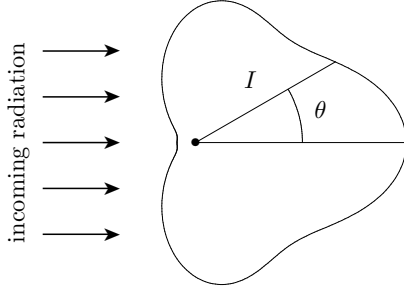


Fig. 3. Scattering diagram of light with $\lambda = 580 \text{ nm}$ impinging on the dust particle with $R = 0.168 \mu\text{m}$. This particle gives the maximal dimensionless efficiency factor for the radiation pressure averaged over the stellar spectrum. For $x_M = 2\pi R/\lambda < 1.38$ scattering is predominantly back to the source. Considered situation corresponds to $x_M \approx 1.820$ and the scattering diagram has the usual preponderance of forward radiation over back radiation (van de Hulst 1981).

the temperature of the dust grain, and T_i is the temperature of the i th gas component. s_i in Eq. (6) is the molecular speed ratio

$$s_i = \sqrt{\frac{m_i}{2kT_i}} U. \quad (7)$$

Here, m_i is the mass of the neutral atom in the i th gas component, k is Boltzmann's constant, and $U = |\mathbf{v} - \mathbf{v}_F|$ is the relative speed of the dust particle with respect to the gas. For the collision parameter γ_i in Eq. (5) we obtain

$$\gamma_i = n_i \frac{m_i}{m} A', \quad (8)$$

where n_i is the concentration of the i th kind of interstellar neutral atom.

2.5. Equation of motion

The equation of motion which determines the dynamics of dust particles in an orbit around a star under the action of

the electromagnetic radiation, the stellar wind and ISW is on the basis of Eqs. (1), (3) and (5)

$$\frac{d\mathbf{v}}{dt} = -\frac{\mu}{r^2} (1 - \beta) \mathbf{e}_R - \frac{\mu\beta}{r^2} \left(1 + \frac{\eta}{Q'_{\text{pr}}} \right) \left(\frac{\mathbf{v} \cdot \mathbf{e}_R}{c} \mathbf{e}_R + \frac{\mathbf{v}}{c} \right) - \sum_{i=1}^N c_{Di} \gamma_i |\mathbf{v} - \mathbf{v}_F| (\mathbf{v} - \mathbf{v}_F), \quad (9)$$

here also the approximation mentioned after Eq. (4) was considered.

2.6. Distance to termination shock

The interaction of the stellar wind with the ISM gas will create a termination shock in the stellar wind. The termination shock in the Solar system was directly observed by *Voyager 1* at a heliocentric distance 94 AU in 2004 and by *Voyager 2* at 84 AU in 2007 (Richardson et al. 2008). The stellocentric distance to the termination shock can be estimated as a distance at which a ram pressure of supersonic stellar wind is equal to pressure caused by the ISM gas (e.g. Holzer 1989; Lee et al. 2009). To match the observed shape of swept-back structure using the interaction with the ISM gas described by Eq. (5) is necessary to use high densities, high speed and/or high temperature of the ISM gas. Therefore for a typical interstellar magnetic field ($\sim 3 \mu\text{G}$) the magnetic pressure in the case of HD 61005 can be neglected. In this case the stellocentric distance to the termination shock r_{TS} can be calculated from

$$\frac{\rho_{\text{sw}} u_{\text{sw}}^2}{r_{\text{TS}}} \approx (n_{\text{H}} + n_{\text{He}} + 2n_{\text{p}}) kT + (m_{\text{H}} n_{\text{H}} + m_{\text{He}} n_{\text{He}} + m_{\text{p}} n_{\text{p}}) v_{\text{F}}^2. \quad (10)$$

Here, ρ_{sw} and u_{sw} are the density and the speed of the stellar wind at the distance 1 AU from star. n_{H} , n_{He} and n_{p} are concentrations of interstellar hydrogen, helium and plasma, respectively. T is the temperature of the interstellar gas unaffected by the interaction with the stellar wind. m_{H} , m_{He} and m_{p} are masses of hydrogen, helium and proton, respectively. A contribution of plasma electrons to the ram pressure of the ISM gas is neglected.

2.7. Initial conditions

We will assume that the source of dust particles forming the swept-back structure at HD 61005 is in the circumstellar ring observed also in the scattered light. As the source of dust particles we consider parent bodies in elliptical orbits with the semimajor axes distributed randomly between 55 and 65 AU. We assume that the elliptical orbits have randomly distributed eccentricities smaller than 0.1. Inclinations of the orbits are distributed randomly between 0 and 2° . Arguments of pericenters, longitudes of ascending nodes and true anomalies of the parent bodies are distributed randomly between 0 and 2π . The dust particle after an ejection from the parent body is subjected to the radiation of the star. The position and velocity in a moment of the ejection can be used in order to calculate initial orbital elements of the dust particle. After the ejection central Keplerian acceleration from the star is reduced by a factor $1 - \beta$ (see text after Eq. 4) and the particle obtains different oscular orbit.

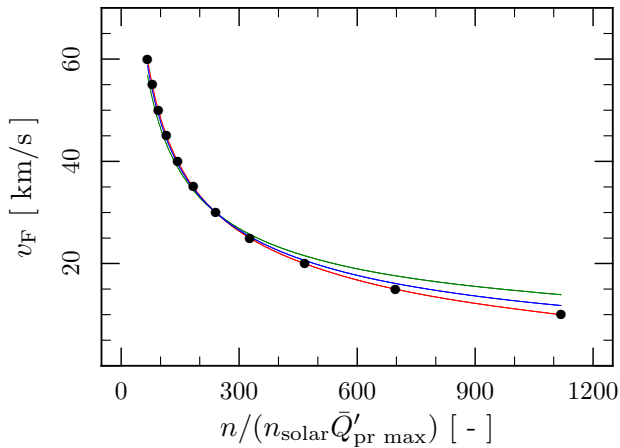


Fig. 4. Relation between the interstellar gas speed and the interstellar gas densities divided by maximal averaged efficiency factor for the radiation pressure (red lines) that give the observed morphology at HD 61005. Used interstellar gas densities at the Sun are $n_{\text{H Sun}} = 0.2 \text{ cm}^{-3}$, $n_{\text{He Sun}} = 0.015 \text{ cm}^{-3}$ and $n_{\text{p Sun}} = 0.032 \text{ cm}^{-3}$. The green line shows pure Stark approximation. The blue line shows the Stark approximation with considered dependence of the drag coefficients on the velocity of the ISM gas.

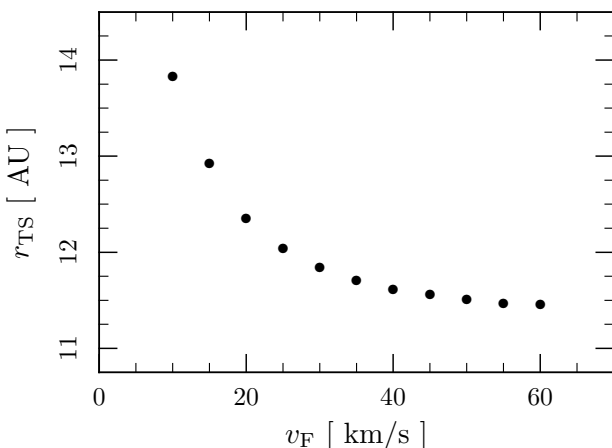


Fig. 5. Distances to the stellar wind termination shock obtained using Eq. (10) giving the observed shape morphology for the dust particles with $Q'_{\text{pr max}} = 1.663$ (see Fig. 4). Calculated distances to the stellar termination shock are much lower than the stellocentric distances 55–65 AU at which the bulk of the debris ring ejecting the dust particles is located. Therefore, the stellar wind should not affect the dynamics of dust particles.

The observed swept-back structure at HD 61005 can be explained with dust particles moving in hyperbolic orbits. The dust particles in the hyperbolic orbits have been observed also in the Solar system and are called β -meteoroids (Zook & Berg 1975). Calculation of initial orbital elements after an ejection to the hyperbolic orbit is shown in Appendix A.

Properties of the star HD 61005 are sufficiently well known. Unfortunately, this cannot be said about properties of the ISM gas which varies the dynamic of the observed dust. After few numerical solutions of the equation of motion is easily to see that observed structure requires the acceleration caused by the ISM to be dominant in the dynamics of ejected dust particles. The dominance can be

accomplished by high density, high speed and/or high temperature of the ISM gas. The high temperature possibility alone requires the ISM gas temperatures more than 10^5 K and for such high temperatures at HD 61005 there is no observational evidence. Therefore, we consider only two remaining possibilities.

In order to obtain observed structure we used number densities for hydrogen, helium and plasma in the same ratios as number densities of the ISM incoming to the Solar system. We have adopted the following number densities $n_{\text{H Sun}} = 0.2 \text{ cm}^{-3}$, $n_{\text{He Sun}} = 0.015 \text{ cm}^{-3}$ and $n_{\text{p Sun}} = 0.032 \text{ cm}^{-3}$ for interstellar hydrogen, helium and plasma entering the Solar system (Frisch et al. 2009). Temperatures of all ISM gas components were equal to $T = 6300 \text{ K}$ which is approximately the temperature of interstellar helium entering the Solar system that is a gas component weakly affected in the interaction of the ISW with the stellar wind. We assumed that the ISM atoms are specularly reflected at the surfaces of the dust grains ($\delta_i = 1$ in Eq. 6).

2.8. Observations in scattered light

We numerically solved the equation of motion for 2×10^5 particles. Obtained trajectories were accumulated into 2D grid observed from a given direction. Similar technique was used also by Debes et al. (2009) and earlier for visualisation of resonant structures in debris disks by Liou & Zook (1999), Moro-Martín & Malhotra (2002), Stark & Kuchner (2008) and others. This technique enables visualisation of an optical depth in a given element of the grid. In order to compare our model with observations of dust in the scattered light we calculated an intensity of light from HD 61005 scattered on each dust particle in the given element of the grid to the observed direction using Mie scattering theory (e.g. Mie 1908; van de Hulst 1981) with an assumption that the light travel through optically thin environment. Mie theory represents one solution of Maxwell's equations for boundary conditions used in our model.

3. Results

By numerical solving of equation of motion one can easily found various properties of the ISM that lead to practically identical resulting shape morphology. It is impossible using today observational data to decide which properties really belong to the ISM gas at HD 61005. Instead of saying that only one properties satisfy we focus on groups of properties which give the observed structure using our dynamical model. Relative speed of HD 61005 with respect to the Sun determined using its measured proper motion is 27.0 km/s . The ISM in the Solar System arrives from the direction $\lambda_{\text{ecl}} = 254.7^\circ$ (heliocentric ecliptic longitude) and $\beta_{\text{ecl}} = 5.2^\circ$ (heliocentric ecliptic latitude) and moves with a speed $v_F = 26.3 \text{ km/s}$ (Lallement et al. 2005). If the Sun and the HD 61005 would be embedded in the same interstellar cloud, the speed of the ISM gas at HD 61005 should be only 12.8 km/s . The ISM with such a small speed requires large densities of the ISM gas in order to create the observed morphology (see further). Therefore, it is more probable that the Sun and the HD 61005 are not embedded in the same interstellar cloud.

3.1. ISW velocity perpendicular to debris ring plane

In Fig. 1 is depicted obtained shape morphology consistent with the observed morphology at HD 61005. The interstellar gas velocity is perpendicular to the debris ring. We have chosen the speed of the ISM $v_F = 30$ km/s and the found densities are $n_H = 80$ cm $^{-3}$, $n_{He} = 6$ cm $^{-3}$ and $n_p = 12.8$ cm $^{-3}$ for interstellar hydrogen, helium and plasma, respectively. In the plots are used Cartesian coordinates with the origin in the star. The bottom-left plot is created by a rotation of a viewpoint in the top-left plot by the angle 45° counterclockwise around x -axis in yz -plane. The bottom-right plot is created by the rotation of a viewpoint in the top-left plot by the angle 95.7° counterclockwise around x -axis in yz -plane in order to show the shape morphology observed from the Earth (Buenzli et al. 2010). The dominance of the acceleration caused by the ISM gas enables to use only single particle size for a creation of correct morphology shape for the given ISM parameters. In this case the shape of swept-back structure is not function of the particle's radius R . This can be proved also analytically using simplifying approximation that the acceleration of the dust particle sufficiently far from the star is given only by Stark approximation. In the Stark approximation the acceleration caused by the ISM gas depends on the velocity as Cv_Fv_F , where C is a constant (see Pástor 2012a). However, the shape of swept-back structure is function of \bar{Q}'_{pr} . The boundary, determining the curvature of “wings”, is formed by dust particles that are most significantly influenced by the stellar radiation. Hence, the particles with maximal \bar{Q}'_{pr} obtained from Mie scattering theory. These particles obtain maximal variation of the velocity in approximately radial direction close to the star. The maximal \bar{Q}'_{pr} is obtained for totally reflecting particles. For the effective temperature of the star 5500 K we can calculate the particle's radius for which $\bar{Q}'_{pr \max}$ is obtained. The obtained radius is 0.168 μ m and corresponding maximal \bar{Q}'_{pr} is 1.663 (Fig. 2). Slightly larger radius about 0.2 μ m for the scattering particles has been suggested from observations by Hines et al. (2007). For this radius we obtain $\bar{Q}'_{pr} = 1.642$ and that is not far from the $\bar{Q}'_{pr \max}$. Fig. 1 was obtained using icy dust particles with radius $R = 0.168$ μ m. In Eq. (2) these parameters give $\beta \approx 3$ for the stellar parameters of HD 61005. Scattering intensities were obtained at $\lambda = 580$ nm. This wavelength is free of any major Farnhofer absorption lines in the solar spectrum. The positions of dust particles are not significantly dependent on wavelength of the observed scattered light. Therefore, the shape morphology should be not depended of chosen wavelength of scattered visible light. Scattering intensities obtained using Mie theory should be exactly correct for the used model. Scattering diagram for the used particle at 580 nm is shown in Fig. 3.

3.2. Speeds and densities of the ISW

The acceleration caused by the ISM gas has such a form that smaller velocity and larger densities of the ISM gas can give the same resulting shape morphology as a larger velocity and smaller densities. In Fig. 4 are shown velocity and densities of the ISM that produce the observed shape of the swept-back structure at HD 61005 using presented model for the dust particles with given $\bar{Q}'_{pr \max}$. The red line is obtained from numerical solution of the equation

of motion (Eq. 9) using a spline interpolation applied on the measured values (black circles). The shape depicted in Fig. 1 corresponds to the ratio for the number densities $n/(n_{Sun}\bar{Q}'_{pr \max}) \approx 240$ on the red line. The observed shape morphology can be obtained with density ratios smaller than 240 for dust particles with $\bar{Q}'_{pr \max} < 1$ at the ISW speed 30 km/s. The green line shows the Stark approximation. The Stark approximation is very crude at small velocities of the ISM gas due to dependence of c_D and U on the velocity of the dust grain. The blue line shows relation $\sum_{i=1}^3 c_{0i}n_im_iv_F^2/\bar{Q}'_{pr \max} = \text{constant} \approx 1.1567 \times 10^{-10}$ kg.m $^{-1}$.s $^{-2}$, where $c_{0i} = c_{Di}(s_{0i})$ and $s_{0i} = \sqrt{m_i/2kT_i} v_F$. The dependence of c_D on the velocity of the ISM gas is considered in this approximation. The solution of the equation of motion is approximated fairly well by both simplified relations. The plots depicting the simplified relations were obtained only with the acceleration from the ISM gas. This demonstrate already mentioned dominance of the ISM gas in the dynamical evolution of the dust particles farther from the star. The star's gravity and the PR effect can be neglected in comparison with influence of the ISM gas farther from the star.

In Debes et al. (2009) speed 25 km/s was used for the interstellar gas. Using depicted results in Fig. 4 we obtain the same observed morphology for dust particles with $\bar{Q}'_{pr \max} = 1$ at densities $n_H \approx 65.4$ cm $^{-3}$, $n_{He} \approx 4.9$ cm $^{-3}$ and $n_p \approx 10.5$ cm $^{-3}$. The model picture in Debes et al. (2009) was obtained with n_H 100 cm $^{-3}$. We found that such high densities of hydrogen alone are not necessary due to three reasons. 1) Debes et al. (2009) used an assumption “that the grains originate from radii ~ 10 AU from the star” Debes et al. (2009, p. 324). In year 2009 shape of the debris ring was not yet determined. The parent bodies on such orbits produce dust particles with much larger initial velocities than the parent bodies in the observed debris ring between 55 and 65 AU. The dust particle moving with such a large initial tangential velocity requires much intensive acceleration from the ISW to be pushed up from the ring plane sufficiently fast. 2) The acceleration in Debes et al. (2009) has different form of the drag coefficient. For the same dust particle, the same hydrogen density and the relative particle-gas speed 25 km/s we obtain that the acceleration in this paper is ~ 1.40 times larger than the acceleration in Debes et al. (2009) at the temperature of hydrogen 6300 K. 3) It is very probable that in the interstellar matter at HD 61005 are also another gas components not only the hydrogen.

If the curvature of swept-back structure would be observed farther from the star, then should be possible to determine densities of ISM components directly. Data in Fig. 4 were fitted to match available observations from Schneider et al. (2014) to distance 230 AU along disk mid-plane with correct distance scaling from Buenzli et al. (2010).

3.3. Interaction of the ISW with stellar wind

In Fig. 5 are shown estimated distances to the stellar wind termination shock calculated using Eq. (10) for densities and speeds corresponding in Fig. 4 to the dust particle with $\bar{Q}'_{pr \max} = 1.663$. The equilibrium between the ram pressure of supersonic stellar wind and the pressure caused by the ISM gas places the termination shock on stellocentric distances much smaller than that of the debris ring. Since we assume that the dust particles originate in the debris ring in

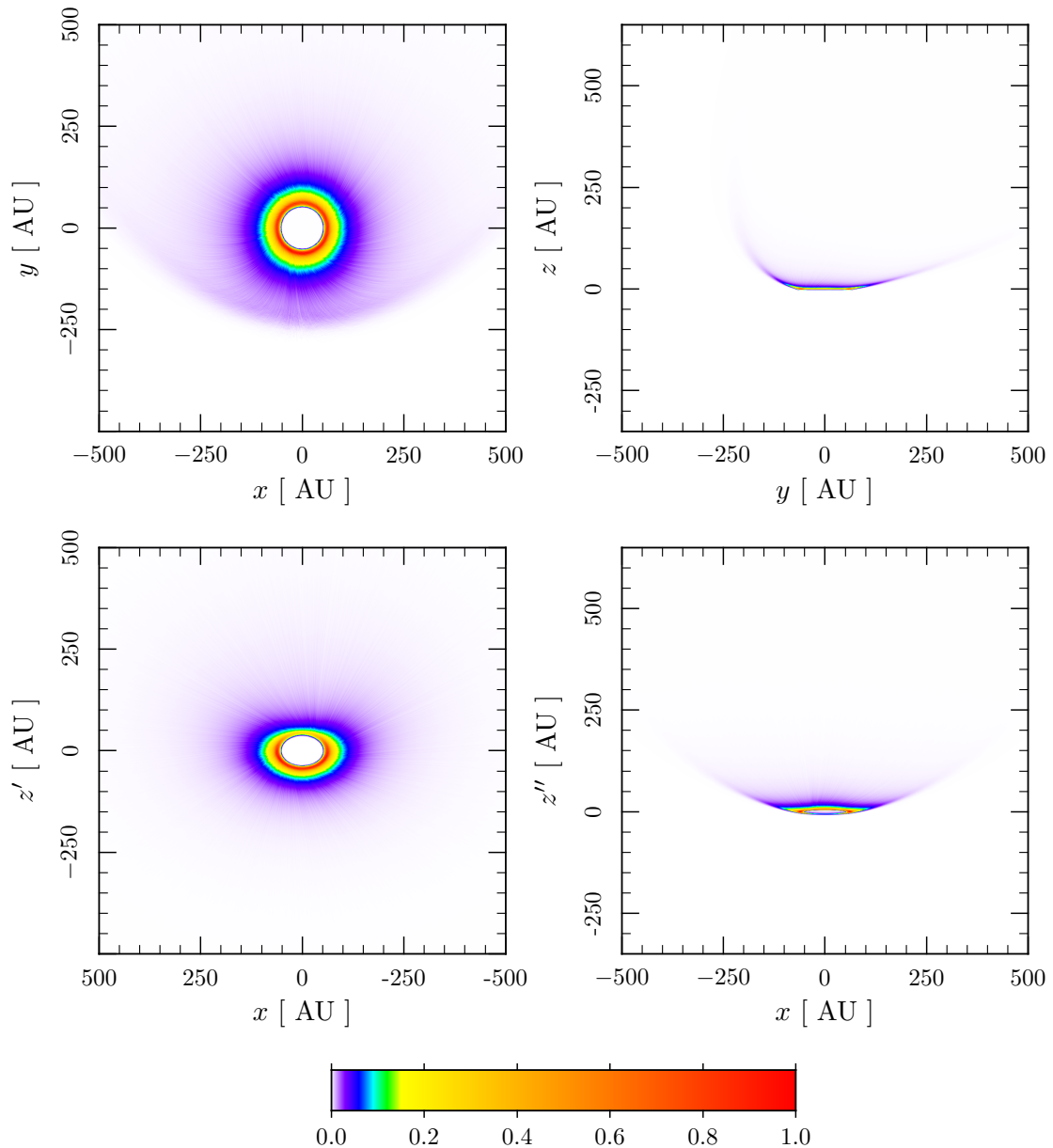


Fig. 6. The same situation as in Fig. 1 only with different interstellar gas velocity vector and different viewpoints. The interstellar gas velocity vector lies in the xz -plane and has 45° angle between its direction and debris ring axis. Its magnitude was modified using Eq. (11) in order to obtain the same observed morphology from the Earth. The bottom-left plot shows the view on the star against the ISW. The bottom-right plot shows the view from the Earth with the same orientation as in Fig. 1.

this case the acceleration caused by the stellar wind can be ignored. However, it is questionable if the swept-back structure is not located on a bow shock of the stellar wind-ISM gas interaction at HD 61005. On the bow shock the ISM gas density should be higher in comparison with a density of the ISM gas that is unaffected by the interaction with stellar wind (e.g. Pogorelov et al. 2006). To find the location of the bow shock a numerical solution of magnetohydrodynamical (MHD) equations is required. If the swept-back structure is located on the bow shock, then also the motion of dust particles should be affected by the acceleration caused by the ISM gas with densities and velocities obtained from the MHD solution. Since the obtained stellocentric distances to the termination shock are far inside of the debris ring the

swept-back structure is probably not located on the bow shock.

3.4. ISW velocity tilted from debris ring axis

The interstellar matter velocity vector may not be perpendicular to the debris ring. Such a configuration can also produce what we observe at HD 61005. Fig. 6 shows obtained shape morphology for the case with the angle between the ISM velocity vector and the debris ring axis is 45° . The ISM velocity vector lies in the plane comprising the line of sight and the ring axis. The bottom-left plot depicts the view against the ISW with the star in the center. The bottom-right plot is created by the rotation of the viewpoint in the top-left plot by angle 95.7° around x -axis counterclockwise

in the yz -plane in order to show the shape morphology observed from the Earth similarly to Fig. 1. We have used the same number densities of the ISM gas components as in Fig. 1. However, simple usage of the same speed of the ISM does not give the observed morphology. To match observed morphology at this tilt of the ISM velocity vector with respect to the debris ring axis the speed must be increased. Using the same approximation as for the independence of observed morphology on the particle's radius we can derive an equation which gives how the speed of the ISM should be modified in order to obtain the same observed morphology. The obtained equation is

$$\frac{v_{\text{FB}}^2 \sum_{i=1}^N c_{0iB} n_{iB} m_{iB}}{v_{\text{FA}}^2 \sum_{i=1}^N c_{0iA} n_{iA} m_{iA}} \approx \frac{\sin \delta_A}{\sin \delta_B}, \quad (11)$$

where the subscripts A and B refer to two different configurations with the ISM velocity vector lying in the plane comprising the line of sight and the ring axis and δ_A is an angle between the line of sight and the ISM velocity in the configuration A.

When the ISM velocity vector is tilted with respect to ring axis, the symmetry between the left and right “wing” observed from the plane comprising the ISM velocity vector and the ring axis is slightly affected. The slope of “wings” slightly depend on that whether the motion of parent bodies in the debris ring is prograde or rectograde. This is caused by the fact components of the initial dust velocity parallel and perpendicular to the ISM velocity vector vary along the mid-plane of the debris ring.

4. Conclusion

We have investigated influence of ISW on a shape morphology of observed swept-back structure originating in the debris ring at HD 61005. For explanation of the observed morphology high velocities or densities of interstellar gas are required. On the boundary of the swept-back structure the dust particles that are maximally influenced by stellar radiation should be present. When paper by Debes et al. (2009) was published no observations of the debris ring producing the dust particles existed. Assumed stellocentric distances about 10 AU used for the location of debris ring were much lower in comparison with today real observed values 55-65 AU. Unfortunately, we were not able to reproduce Debes et al. (2009) results using the debris ring at 10 AU interacting with interstellar hydrogen with density $n_{\text{H}} = 100 \text{ cm}^{-3}$. Probably low assumed stellocentric distance together with other reasons (see Sect. 3.2) led to higher initial velocities of dust particles and consequently to higher densities and velocities of ISW required for a creation of the observed shape. Required density for ISM with speed 25 km/s is 327.1 times higher than ISM entering the Solar system in comparison with value 500 in Debes et al. (2009). For such a strong ISW the stellar wind termination shock should be inside the debris ring.

Observed shape can be obtained also in the case when ISW is not perpendicular on the ring plane. Suitable configuration exists also in the case when the ISW velocity lies in a plane which comprise the line of sight and the debris ring axis. Simple relation between suitable ISM speed and the angle between the line of sight and ISM velocity can be obtained.

In general, we can conclude that observed morphology created by the dust originating in the debris ring at HD 61005 can be explained if we consider dust under the action of ISW.

References

- Baines, M. J., Williams, I. P., Asebiomo, A. S. 1965, MNRAS, 130, 63
- Buenzli, E., Thalmann, C., Vigan, A., et al. 2010, A&A, 524, L1
- Debes, J. H., Weinberger, A. J., Kuchner, M. J. 2009, ApJ, 702, 318
- Desidera, S., Covino, E., Messina, S., et al. 2011, A&A, 529, A54
- Esposito, T. M., Fitzgerald, M. P., Graham, J. R., et al. 2016, AJ, 152, 85
- Frisch, P. C., Bzowski, M., Grün, E., et al. 2009, Space Sci. Rev., 146, 235
- Gustafson, B. A. S. 1994, Annu. Rev. Earth Planet. Sci., 22, 553
- Holzer, T. E. 1989, Annu. Rev. Astron. Astrophys., 27, 199
- Hines, D. C., Schneider, G., Hollenbach, D., et al. 2007, ApJ, 671, L165
- van de Hulst, H. C. 1981, Light Scattering by Small Particles (Dover Publications, New York)
- Johnstone, C. P., Güdel, M., Brott, I., Lüftinger, T. 2015, A&A, 577, A28
- Klačka, J. 1992, Earth, Moon, Planets, 59, 41
- Klačka, J. 2004, Celest. Mech. Dyn. Astron., 89, 1
- Klačka, J., Petržala, J., Pástor, P., Kómar, L. 2012, MNRAS, 421, 943
- Klačka, J., Petržala, J., Pástor, P., Kómar, L. 2014, Icarus, 232, 249
- Lallement, R., Quémerais, E., Bertaux, J. L., et al. 2005, Science, 307, 1447
- Lee, M. A., Fahr, H. J., Kucharek, H., et al. 2009, Space Sci. Rev., 146, 275
- van Leeuwen, F. 2007, A&A, 474, 653
- Liou, J.-Ch., Zook, H. A. 1999, AJ, 118, 580
- Maness, H. L., Kalas, P., Peek, K. M. G., et al. 2009, ApJ, 707, 1098
- Matt, S. P., MacGregor, K. B., Pinsonneault, M. H., Greene, T. P. 2012, ApJ, 754, L26
- Mie, G. 1908, Ann. Phys., 25, 377
- Moro-Martín, A., Malhotra, R. 2002, AJ, 124, 2305
- Olofsson, J., Samland, M., Avenhaus, H., et al. 2016, A&A, 591, A108
- Pallavicini, R., Golub, L., Rosner, R., et al. 1981, ApJ, 248, 279
- Pástor, P. 2012a, Celest. Mech. Dyn. Astron., 112, 23
- Pástor, P. 2012b, MNRAS, 426, 1050
- Pástor, P., Klačka, J., Kómar, L. 2011, MNRAS, 415, 2637
- Poynting, J. M. 1904, Philos. Trans. R. Soc. Lond., Ser. A, 202, 525
- Pogorelov, N. V., Zank, G. P., Ogino, T. 2006, ApJ, 644, 1299
- Richardson, J. D., Kasper, J. C., Wang, C., Belcher, J. W., Lazarus, A. J. 2008, Nature, 454, 63
- Robertson, H. P. 1937, MNRAS, 97, 423
- Siess, L., Dufour, E., Forestini, M. 2000, A&A, 358, 593
- Scherer, K. 2000, J. Geophys. Res., 105, A5, 10329
- Schneider, G., Grady, C. A., Hines, D. C., et al. 2014, AJ, 148, 59
- Stark, C. C., Kuchner, M. J. 2008, ApJ, 686, 637
- Torres, C. A. O., Quast, G. R., Melo, C. H. F., Sterzik, M. F. 2008, Young Nearby Loose Associations, in Handbook of Star Forming Regions, Volume II: The Southern Sky, ed. Reipurth B. (ASP Monograph Publications), arXiv:0808.3362
- Wright, N. J., Drake, J. J., Mamajek, E. E., Henry, G. W. 2011, ApJ, 743, 48
- Zook, H. A., Berg, O. E. 1975, Planet. Space Sci., 23, 183

Appendix A: Initial elements after an ejection to hyperbolic orbit

The positions and velocities of the parent body and the particle in a moment of the ejection with zero ejection velocities are equal. After an ejection from a parent body in an elliptical orbit the semimajor axis of the particle orbit can be calculated as follows. For the parent body we have

$$\frac{v^2}{2} - \frac{\mu}{r} = -\frac{\mu}{2a_p}, \quad (\text{A.1})$$

where v is the speed in the moment of ejection and a_p is the semimajor axis of the parent body. The subscript p will be used for quantities belonging to the parent body. For dust particle with $\beta > 1$ ejected to a hyperbolic orbit we have

$$\frac{v^2}{2} - \frac{\mu(1-\beta)}{r} = -\frac{\mu(1-\beta)}{2a}. \quad (\text{A.2})$$

The substitution of $v^2/2$ from Eq. (A.1) to Eq. (A.2) gives for the semimajor axis of the hyperbolic orbit

$$a = \frac{(\beta-1)a_p}{2\beta\frac{a_p}{r} - 1}. \quad (\text{A.3})$$

Comparison of the angular momentum H written using the orbital elements of the parent body and the particle in the moment of ejection gives

$$\begin{aligned} H &= |\mathbf{r} \times \mathbf{v}| = \sqrt{\mu a_p (1 - e_p^2)} \\ &= \sqrt{\mu a (\beta - 1) (e^2 - 1)}. \end{aligned} \quad (\text{A.4})$$

If we substitute Eq. (A.3) to Eq. (A.4), then we can determine the eccentricity of the hyperbolic orbit

$$e^2 = 1 + \frac{a_p (1 - e_p^2)}{a (\beta - 1)}. \quad (\text{A.5})$$

The particle moves in the same plane as the parent body after the ejection with the zero ejection velocity. Hence, the ascending nodes and inclinations are equal

$$\Omega = \Omega_p, \quad i = i_p. \quad (\text{A.6})$$

In the moment of ejection are true longitudes of the parent body and the particle equal. Therefore

$$f + \omega = f_p + \omega_p, \quad (\text{A.7})$$

here f is the true anomaly and ω is the argument of pericenter. For stellocentric distance of the dust particle with $\beta > 1$ on the hyperbolic orbit we have

$$r = \frac{a(e^2 - 1)}{e \cos f - 1}. \quad (\text{A.8})$$

Radial components of velocities of the parent body (v_{Rp}) and the particle (v_R) are equal in the moment of ejection

$$\begin{aligned} v_{Rp} &= \sqrt{\frac{\mu}{a_p(1 - e_p^2)}} e_p \sin f_p \\ &= \sqrt{\frac{\mu(\beta - 1)}{a(e^2 - 1)}} e \sin f = v_R, \end{aligned} \quad (\text{A.9})$$

From the equality of transversal components of the velocities we obtain

$$\begin{aligned} v_{Tp} &= \sqrt{\frac{\mu}{a_p(1 - e_p^2)}} (1 + e_p \cos f_p) \\ &= \sqrt{\frac{\mu(\beta - 1)}{a(e^2 - 1)}} (e \cos f - 1) = v_T. \end{aligned} \quad (\text{A.10})$$

Using Eq. (A.4) in Eqs. (A.9) and (A.10) we can calculate the true anomaly

$$e \sin f = \frac{e_p \sin f_p}{\beta - 1}, \quad e \cos f = \frac{\beta + e_p \cos f_p}{\beta - 1}. \quad (\text{A.11})$$

The true anomaly substituted in Eq. (A.7) determine the argument of pericenter. For particles with $\beta \approx 3$ released from parent bodies with nearly circular orbits ($e_p \approx 0$) the true anomaly is always close to zero, in other words, particle is ejected close to the pericenter of the hyperbolic orbit.